J. Fluid Mech. (2019), *vol.* 874, *pp.* 263–284.
doi:10.1017/jfm.2019.405

Turbulent temperature fluctuations in a closed Rayleigh–Bénard convection cell

Yin Wang[1], **Xiaozhou He**[2] **and Penger Tong**[1,†]

[1]Department of Physics, Hong Kong University of Science and Technology, Clear Water Bay, Kowloon, Hong Kong

[2]School of Mechanical Engineering and Automation, Harbin Institute of Technology, Shenzhen, China

(Received 18 January 2019; revised 7 May 2019; accepted 8 May 2019;
first published online 4 July 2019)

We report a systematic study of spatial variations of the probability density function (PDF) $P(\delta T)$ for temperature fluctuations δT in turbulent Rayleigh–Bénard convection along the central axis of two different convection cells. One of the convection cells is a vertical thin disk and the other is an upright cylinder of aspect ratio unity. By changing the distance z away from the bottom conducting plate, we find the functional form of the measured $P(\delta T)$ in both cells evolves continuously with distinct changes in four different flow regions, namely, the thermal boundary layer, mixing zone, turbulent bulk region and cell centre. By assuming temperature fluctuations in different flow regions are all made from two independent sources, namely, a homogeneous (turbulent) background which obeys Gaussian statistics and non-uniform thermal plumes with an exponential distribution, we obtain the analytic expressions of $P(\delta T)$ in four different flow regions, which are found to be in good agreement with the experimental results. Our work thus provides a unique theoretical framework with a common set of parameters to quantitatively describe the effect of turbulent background, thermal plumes and their spatio-temporal intermittency on the temperature PDF $P(\delta T)$.

Key words: Bénard convection, turbulent convection, turbulent mixing

1. Introduction

Mixing of a passive scalar field, such as temperature or concentration, by a chaotic velocity field is a common phenomenon in nature and technology. It is relevant to many practical applications ranging from transport and chemical reactions to design and operation of mixing equipment in various industrial processes of polymers, minerals, fine chemicals, paints, cosmetics, food, water and waste water treatment (Ottino 1989; Paul, Atiemo-Obeng & Kresta 2004; Dimotakis 2005). When the fluid motion is turbulent, the repeated action of advection and stretching is known to create convoluted spatial structures, characterized by elongated lamellae (in two dimensions) or sheets (in three dimensions) with a wide range of self-similar scales, which promote mixing for diffusive transfer at the smallest length scale and reduction

† Email address for correspondence: penger@ust.hk

of mixing times (Ottino 1989; Sreenivasan, Ramshankar & Meneveau 1989; Procaccia *et al.* 1991; Villermaux 2012). In the past decades, there has been a large number of theoretical (Procaccia & Zeitak 1989, 1990; She & Orszag 1991; Sreenivasan 1991; Grossmann & Lohse 1992; Benzi *et al.* 1993; Grossmann & Lohse 1993; She & Léveque 1994; Chertkov *et al.* 1995; Gawędzki & Kupiainen 1995; Shraiman & Siggia 1995*a*,*b*; Cao & Chen 1997; Ching & Chau 2001; Ching 2007; Arnèodo *et al.* 2008), numerical (Cao, Chen & Sreenivasan 1996; Kerr 1996; Calzavarini, Toschi & Tripiccione 2002; Camussi & Verzicco 2004; Ching, Guo & Lo 2008) and experimental (Wu *et al.* 1990; Procaccia *et al.* 1991; Solomon & Gollub 1991; Tong & Shen 1992; Benzi *et al.* 1994; Cioni, Ciliberto & Sommeria 1995; Takeshita *et al.* 1996; Ashkenazi & Steinberg 1999; Zhou & Xia 2001; Skrbek *et al.* 2002; Mashiko *et al.* 2004) studies of small-scale velocity and temperature fluctuations in turbulent flows. Details about these studies have been reviewed by Sreenivasan (1991), Siggia (1994), Warhaft (2000), Biferale & Procaccia (2005), Ishihara, Gotoh & Kaneda (2009), Lohse & Xia (2010), Chillá & Schumacher (2012).

Many experimental studies focused on the structure functions, $\langle \delta T_r^n \rangle$, of temperature increment $\delta T_r = T(x+r) - T(x)$ between two points separated by a distance r, aimed at testing the anomalous scaling (He, Shang & Tong 2014). Some of the experiments were carried out in turbulent Rayleigh–Bénard convection (RBC) (Siggia 1994; Kadanoff 2001; Lohse & Xia 2010), in which a confined fluid layer of thickness H is heated from below and cooled from the top with a constant vertical temperature gradient parallel to gravity. When the temperature difference ΔT across the fluid layer or its dimensionless expression, the Rayleigh number Ra, is sufficiently large, the bulk fluid becomes turbulent and heat is transported predominantly by convection. In addition to the study of the intermittent behaviour of temperature increment δT_r, the study of amplitude fluctuations of the local temperature at a fixed point is also of great interest. For example, an intriguing feature of RBC is the continuing appearance of large fluctuations in the temperature field, which do not follow the Gaussian statistics (Kadanoff 2001). Instead, the measured probability density function (PDF) $P(\delta T)$ of temperature fluctuations δT from the local mean value was found to have an exponential tail, which falls off much slower than a Gaussian (see figure 5*d*). Such an exponential PDF was observed in a wide dynamic range with Ra varied from 4×10^7 up to 10^{15} and in various convecting fluids, such as low-temperature helium gas (Castaing *et al.* 1988; Sano, Wu & Libchber 1989; Niemela *et al.* 2000), mercury (Gollub *et al.* 1991), sulphur hexafluoride gas (Belmonte, Tilgner & Libchaber 1994), fluorocarbon FC72 (Wei & Ahlers 2016) and water (Du & Tong 2001; Zhou & Xia 2002; He, Tong & Xia 2007).

In a more recent experiment, He, Wang & Tong (2018) showed with solid experimental evidence that the exponential PDF in RBC is generated by the thermal plumes, which can be uniquely characterized by the local thermal dissipation rate $\epsilon(t) \equiv \kappa[\nabla T(t)]^2$. The thermal plumes are intermittently emitted from the thermal boundary layers (BLs) and carry temperature fluctuations from the BLs to the bulk region of the flow (Siggia 1994; Kadanoff 2001). Because of rapid mixing and advection of warm and cold plumes passing through the central region of the convection cell, the local thermal dissipation rate has a broad distribution $f(\epsilon)$ (He & Tong 2009). Owing to this dynamic heterogeneity in ϵ, the temperature PDF $P(\delta T)$ can be written as

$$P(\delta T) = \int_0^\infty G(\delta T|\epsilon) f(\epsilon)\, \mathrm{d}\epsilon, \tag{1.1}$$

where $G(\delta T|\epsilon)$ is the conditional PDF of temperature fluctuations when ϵ is held constant. The measured $G(\delta T|\epsilon)$ was found to be of Gaussian form

$$G(\delta T|\epsilon) = \frac{1}{\sqrt{2\pi}\sigma_T(\epsilon)} e^{-\delta T^2/[2\sigma_T^2(\epsilon)]}, \tag{1.2}$$

and its variance σ_T^2 for different values of ϵ follows an exponential distribution. The convolution of the two distribution functions gives rise to the exponential PDF $P(\delta T)$. This work thus provided a direct link between the coherent structures in the convective flow (thermal plumes) and statistics of local temperature fluctuations.

In this paper, we report a systematic study of spatial variations of the temperature PDF $P(\delta T)$ in two different closed convection cells, which provide a unique spatial distribution of thermal plumes neither homogeneous nor isotropic (Shang *et al.* 2003). This steady-state distribution of thermal plumes and the resulting large-scale velocity field with a single-rotation-roll symmetry allow us to probe distinct changes of the functional form of $P(\delta T)$ in four different flow regions, namely, the thermal boundary layer, mixing zone, turbulent bulk region and cell centre, by moving the temperature probe from the bottom to the centre of the convection cell along its central axis. A central finding of this investigation is that temperature fluctuations in the four flow regions are all made from two independent sources, namely,

$$\delta T(t) = \delta T_B(t) + \delta T_P(t), \tag{1.3}$$

where $\delta T_B(t)$ denotes temperature fluctuations from the (turbulent) background, which obeys Gaussian statistics, and $\delta T_P(t)$ represents those resulting from the thermal plumes with an exponential distribution. As a result, the temperature PDF $P(\delta T)$ is well described by a convolution of the two modes of fluctuations with a relative strength, which varies among the four different flow regions. While the decomposition of fluctuation modes has been proposed in various forms in previous studies (Procaccia *et al.* 1991; Naert *et al.* 1998; Grossmann & Lohse 2004; Wilczek 2016; Le Borgne *et al.* 2017; He *et al.* 2018), it is the first time that these ideas are systematically tested in a well-characterized turbulent system with a solid experimental support.

The remainder of the paper is organized as follows. We first describe the experimental methods in § 2. Experimental results are presented in § 3. Further theoretical analyses are given in § 4. Finally, the work is summarized in § 5.

2. Experiment

The experimental apparatus and procedures used in this experiment are similar to those described previously (He & Tong 2009; Wang, He & Tong 2016; Wang *et al.* 2018*b*), and here we only mention some key points. The experiment is conducted in two convection cells with different geometries. One of them is a vertical thin disk with its circular cross-section aligned parallel to gravity, as shown in figure 1(*a*). The cell has a diameter $D = 188$ mm and thickness $L = 20$ mm, and thus the corresponding aspect ratio is $\Gamma \equiv L/D \simeq 0.1$. The top and bottom 1/3 of the circular side wall are made of copper of 8 mm in thickness. The surface of the copper plates in contact with the convecting fluid is electroplated with a thin layer of nickel. The remaining 1/3 of the side wall on both sides is made of transparent Plexiglas of 18 mm in thickness. The two flat end walls of the cell are also made of the same type of Plexiglas. Two silicon rubber film heaters connected in parallel are sandwiched on the back side of the bottom conducting plate to provide constant and uniform heating. The top

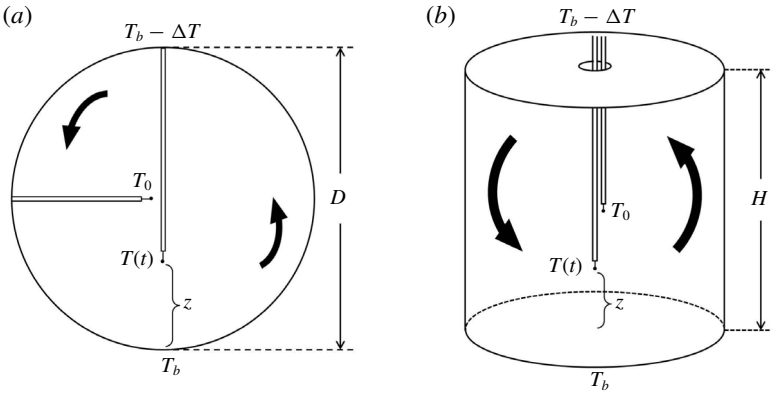

FIGURE 1. Sketch of the experimental set-up for the measurement of local temperature fluctuations at different locations along the central axis of (*a*) the vertical thin disk and (*b*) the $\Gamma = 1$ upright cylinder. The black arrows indicate the direction of the large-scale circulation.

copper plate is in contact with a cooling chamber consisting of two water channels. The temperature of the top plate is maintained by a temperature-controlled circulator (NESLAB, RTE740), which circulates cooling water with a temperature stability of 10 mK. The temperature of the top and bottom plates is measured at a rate of 2 Hz by calibrated thermistors with an accuracy of 5 mK. They are embedded in each plate at a distance of 1 mm away from the surface of the conducting plate. This cell was used in the previous convection experiments (Song, Villermaux & Tong 2011; Wang *et al.* 2016, 2018*a*,*b*).

The second cell is an upright cylinder, as shown in figure 1(*b*). The inner diameter of the cell is $D_{up} = 19.0$ cm and its height is $H = 19.0$ cm. The corresponding aspect ratio of the cell is $\Gamma \equiv D_{up}/H = 1$. The side wall of the cell is made of a transparent Plexiglas ring with a wall thickness of 6 mm. The top and bottom plates of the cell are made of brass and their surfaces are electroplated with a thin layer of gold. The Plexiglas ring side wall is sandwiched between the two plates and is sealed to the top and bottom plates via two rubber O-rings. Except for the difference in shape, all other aspects of the cell, such as the heating (cooling) of the bottom (top) plate and temperature measurement of the conducting plates, remain the same as those for the vertical thin disk. The temperature standard deviation of the top and bottom plates is found to be within 1 % of ΔT used in the experiment. This cell was also used in previous convection experiments (He & Tong 2009; He, Ching & Tong 2011; Wang *et al.* 2018*b*).

In the experiment, the entire convection cell is placed inside a square thermostat box, whose temperature matches the mean temperature of the bulk fluid (maintained at $40 \pm 0.1\,^{\circ}\mathrm{C}$), in order to prevent heat exchange between the convecting fluid and the surroundings. The Rayleigh number Ra for the thin disk is defined as $Ra \equiv \psi g \Delta T D^3/(\nu\kappa)$, where g is the gravitational acceleration, ΔT is the vertical temperature difference across the cell and ψ, ν and κ are, respectively, the thermal expansion coefficient, viscous and thermal diffusivity of the convecting fluid. For the upright cylinder, the cell height H is used to replace D. The Prandtl number Pr is defined as $Pr \equiv \nu/\kappa$. Two working fluids are used in the experiment. For the thin disk, a 20 wt. % aqueous solution of glycerin with $Pr = 7.6$ is used. For the upright

cylinder, both distilled water with $Pr = 4.4$ and the 20 wt. % aqueous solution of glycerin with $Pr = 7.6$ are used. In the experiment, the temperature T_b of the bottom heating plate is varied in the range $42.4 \lesssim T_b \lesssim 60.2\,^{\circ}\mathrm{C}$, and the temperature T_t of the top cooling plate is varied in the range $13.8 \lesssim T_t \lesssim 37.8\,^{\circ}\mathrm{C}$. Correspondingly, Ra is varied in the range $9 \times 10^8 \lesssim Ra \lesssim 1.2 \times 10^{10}$ and Pr is fixed for a given fluid. The black arrows in figure 1 show the direction of the large-scale circulation (LSC). To pin down the azimuthal motion of the LSC in the upright cylinder, the cylindrical cell is tilted slightly at a small angle ($<1^{\circ}$) by adjusting the levelling plate of the cell. It has been shown (Ahlers, Brown & Nikolaenko 2006*a*) that such a small tilt to the $\Gamma = 1$ upright cylinder does not affect the convective flow very much, as the single-roll structure of the LSC is quite stable in the $\Gamma = 1$ cell (Qiu & Tong 2001). The LSC structure in the $\Gamma = 0.5$ upright cylinder, however, is more sensitive to the cell tilt and so are the temperature fluctuations (Chillá *et al.* 2004).

The local fluid temperature is measured using a glass-encapsulated thermistor of diameter 0.17 mm with an accuracy of 5 mK (AB6E3-B05KA202R). Details about the temperature calibration and measurements have been reported elsewhere (He & Tong 2009). To guide the two thermistors into the thin disk, we install a horizontal and a vertical stainless steel tube in the cell, as shown in figure 1(*a*). The horizontal tube is fixed to measure the mean temperature T_0 at the cell centre. The vertical tube is used to measure the temperature time series data $T(t)$ with varying distance z away from the centre of the bottom plate. The vertical tube is mounted on a translational stage, which is controlled by a stepping motor with a position resolution of 50 μm. The measurements of T_0 and $T(t)$ are made, respectively, at the sampling rates of 2 Hz and 15 Hz. Typically, we take 1 h long time series data (5.4×10^4 data points) at each location of z for the measurement of $T(t)$. The measurement of temperature fluctuations in the upright cylinder is made in a similar way, except that a vertical tube is installed to measure T_0, as shown in figure 1(*b*).

3. Experimental results

3.1. *Turbulent temperature fluctuations in the thin disk*

Figure 2(*a*) shows the evolution of the measured local temperature variations $T(t)$ for four different values of distance z away from the centre of the bottom plate, and at a fixed value of $Ra = 5.3 \times 10^9$ and $Pr = 7.6$ in the thin disk. Figure 2(*b*) shows the corresponding PDFs of the measured $T(t)$ in figure 2(*a*). In a recent experiment and direct numerical simulation, we have shown that there is a well-developed thermal BL near the bottom (top) conducting plate of the thin disk cell. A typical value of the BL thickness δ at this Ra is $\delta \simeq 0.55$ mm. Heat transport inside the BL is accomplished mainly by thermal diffusion, which establishes a large mean temperature gradient across the BL. In the region outside the BL, however, heat transport is dominated by turbulent convection and the mean temperature along the central axis of the bulk region is approximately constant. At $z = 0.2$ mm which is in the inner region of the BL, the measured $T(t)$ (black curve in figure 2*a*) reveals large symmetric fluctuations, and thus their PDF (black squares in figure 2*b*) has a symmetric shape with a broad width. In addition, the measured mean temperature $\langle T \rangle$ at this location is much larger than that at the other three positions.

At $z = 4.9$ mm which is outside the BL and in the mixing zone (Wang *et al.* 2016), the measured $T(t)$ (red curve in figure 2*a*) reveals large temperature spikes in one direction, resulting from warm thermal plumes passing through the measuring position. These warm plumes are intermittently emitted from the bottom BL. In addition to the

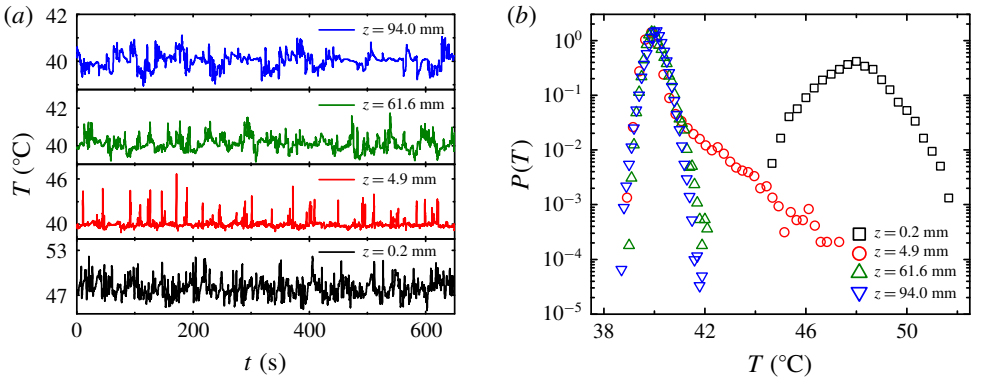

FIGURE 2. (Colour online) (*a*) Evolution of the measured local temperature variations $T(t)$ for 4 different values of distance z away from the centre of the bottom plate (bottom to top): $z = 0.2$ mm (black curve), $z = 4.9$ mm (red curve), $z = 61.6$ mm (green curve) and $z = 94.0$ mm (blue curve). The measurements are made in the thin disk at $Ra = 5.3 \times 10^9$ and $Pr = 7.6$ (20 wt.% aqueous solution of glycerin). (*b*) Corresponding PDFs of the measured $T(t)$ in (*a*) at $z = 0.2$ mm (black squares), $z = 4.9$ mm (red circles), $z = 61.6$ mm (green up triangles) and $z = 94.0$ mm (blue down triangles).

hot spikes, the measured $T(t)$ also shows small continuous fluctuations resulting from the turbulent background. As shown in figure 2(*b*), the intermittent temperature spikes in the time series $T(t)$ give rise to an exponential tail in the corresponding temperature PDF $P(T)$ (red circles with $T \gtrsim 41\,^{\circ}\mathrm{C}$). The small background fluctuations, on the other hand, produce a symmetric peak in the measured $P(T)$.

By increasing z further into the turbulent bulk region, the warm plumes are mixed and dissipated by the flow field. As a result, the intermittent spikes in $T(t)$ and the asymmetric tail in the resulting $P(T)$ gradually diminish. The green curve in figure 2(*a*) and green up triangles in figure 2(*b*) show an example at $z = 61.8$ mm. In addition, the standard deviation of temperature fluctuations also decreases with increasing z. Finally, at the cell centre ($z = 94.0$ mm), the standard deviation of temperature fluctuations becomes the smallest (blue curve in figure 2*a*), and the resulting $P(T)$ shows the smallest width (blue down triangles in figure 2*b*). Because of the reflection symmetry at the cell centre, the measured $P(T)$ has a symmetric shape as expected. An interesting feature shown in figure 2(*b*) is that once outside the thermal BL, both the peak position and left side of the peak of all the measured $P(T)$ remain unchanged with z. This result suggests that temperature fluctuations in the bulk region outside the BL have a fairly uniform turbulent background (Zhou & Xia 2013).

Figure 3 shows a sketch of the four flow regions in the thin disk cell, as discussed above. In particular, the BL can be further divided into two sub-regions: inner and outer regions. In the inner region of the BL ($z \lesssim 0.6\delta$), the mean value of the local temperature decreases linearly with distance z and heat is transported primarily by diffusion. In the outer region of the BL ($0.6\delta \lesssim z \lesssim 2\delta$), the mean value of the local temperature gradually approaches a constant value and thermal plumes start to form. These thermal plumes are emitted intermittently into the mixing zone ($0.01 \lesssim z/D \lesssim 0.1$) outside the BL and then are carried away by the LSC (as marked by the black arrow in figure 3). Because of turbulent mixing and thermal dissipation, the thermal

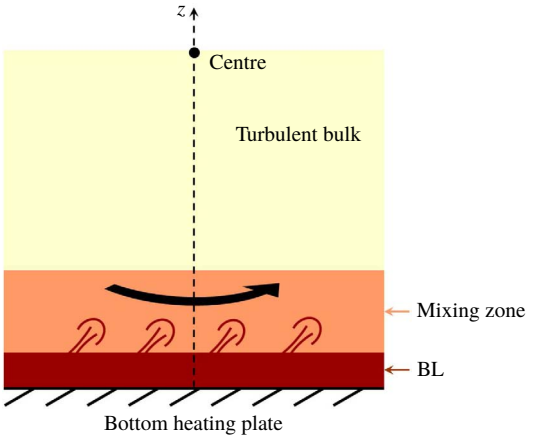

FIGURE 3. (Colour online) Sketch of the four flow regions in the thin disk cell, namely, boundary layer (BL, $z \lesssim 2\delta$), mixing zone ($0.01 \lesssim z/D \lesssim 0.1$), turbulent bulk ($0.1 \lesssim z/D \leqslant 0.5$) and cell centre ($z/D = 0.5$). The vertical dashed line shows the central z-axis of the cell. The BL can be further divided into an inner region ($z \lesssim 0.6\delta$) and an outer region ($0.6\delta \lesssim z \lesssim 2\delta$), in which thermal plumes start to form. The black arrow indicates the direction of the large-scale circulation.

plumes in the turbulent bulk region ($0.1 \lesssim z/D \lesssim 0.5$) become less energetic and fewer in number compared with those in the mixing zone.

We now discuss the scaling properties of the measured PDF $P(\delta T)$ of temperature fluctuations δT from the mean value with varying values of z and Ra. Here $\delta T = T(t) - \langle T \rangle$ with $\langle T \rangle$ being the local mean temperature. It is found that the temperature PDFs obtained at a fixed value of z and different values of Ra can all be brought into coincidence, by normalizing δT by its root mean square (r.m.s.) value σ_T. Plots of $P(\delta T)$ versus $\delta T/\sigma_T$ remain unchanged in the Ra range studied and only σ_T changes with Ra. Figure 4 shows the measured $P(\delta T)$ as a function of $\delta T/\sigma_T$ for different values of Ra in four regions of z. It is seen that the measured $P(\delta T)$ in each region of z has a unique functional form independent of Ra.

Figure 4(a) shows the measured $P(\delta T)$ as a function of normalized temperature fluctuations $\delta T/\sigma_T$ when z is in the inner region of the BL with $z/\delta \lesssim 0.62$, where the mean temperature gradient is almost constant. It is seen that all of the measured PDFs $P(\delta T)$ can be well described by a Gaussian function (dashed line)

$$P(\delta T) = \frac{1}{\sqrt{2\pi}\sigma_T} e^{-\delta T^2/(2\sigma_T^2)}, \tag{3.1}$$

and only σ_T changes with z. For RBC in an rectangular cell, the measured $P(\delta T)$ inside the BL was also found to have a similar Gaussian form (Zhou & Xia 2013). In the outer region of the BL with $0.62 \lesssim z/\delta \lesssim 2$, while plots of $P(\delta T)$ versus $\delta T/\sigma_T$ remain unchanged with Ra at a fixed value of z/δ, the shapes of the measured $P(\delta T)$ for different values of z start to show systematic deviations from the Gaussian function. These deviations cause the measured $P(\delta T)$ to become asymmetric and skewed toward the positive side of $\delta T/\sigma_T$ with the skewness increasing with z.

When z moves beyond the BL region ($z/\delta \gtrsim 2$ or equivalently $z/D \gtrsim 0.01$), the BL thickness δ is no longer the scaling length. Instead, the normalized variance profile

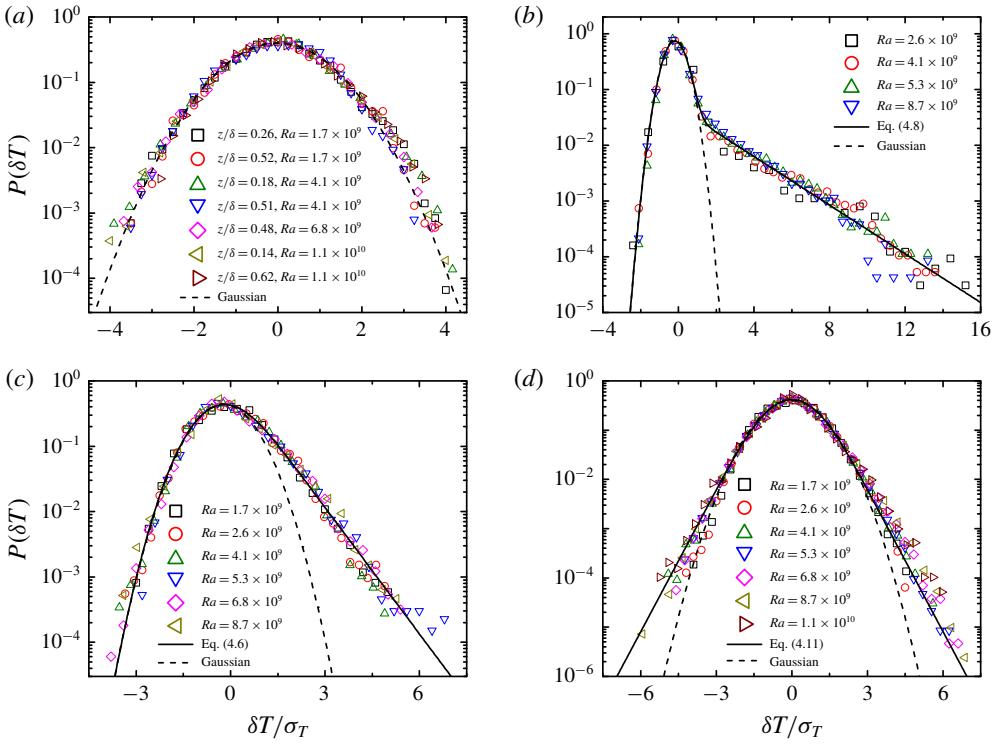

FIGURE 4. (Colour online) Measured PDF $P(\delta T)$ of the normalized temperature fluctuation $\delta T/\sigma_T$ for different values of Ra with a fixed value $Pr = 7.6$ (20 wt. % aqueous solution of glycerin). The measurements are made in the thin disk and in four different regions of distance z away from the bottom plate: (*a*) $z/\delta \lesssim 0.62$ (inner region of the BL), (*b*) $z/D \simeq 0.026$ (mixing zone), (*c*) $z/D \simeq 0.33$ and (*d*) $z/D = 0.5$ (cell centre). The dashed lines in (*a–d*) show the Gaussian function given in (3.1). The solid line in (*b*) shows a fit of (4.8) to the data points with $\alpha_1 = 0.25 \pm 0.05$ and $\beta = 0.1 \pm 0.03$. The solid line in (*c*) shows a fit (4.6) to the data points with $\alpha_1 = 1.1 \pm 0.2$. The solid line in (*d*) is a fit of (4.11) to the data points with $\alpha = 1.7 \pm 0.3$.

$\sigma_T^2(z)/(\sigma_T^2)_0$, with $(\sigma_T^2)_0$ being the maximal value of σ_T^2, was found to scale with z/D in the range $0.01 \lesssim z/D \lesssim 0.1$ (mixing zone) (Wang *et al.* 2016, 2018*b*). Figure 4(*b*) shows an example of the measured $P(\delta T)$ in the mixing zone for different values of Ra. The measurements are made at approximately the same position with $z/D \simeq 0.026$. All of the PDFs collapse onto a single curve, which has a Gaussian-like main portion (dashed line) for small temperature fluctuations ($\delta T/\sigma_T \lesssim 1$) and a long exponential tail for large temperature fluctuations ($\delta T/\sigma_T \gtrsim 2$). As shown in figure 2(*a*) (red curve), the long exponential tail is caused by the warm plumes, which are intermittently emitted from the bottom BL and pass through the measuring position. For other values of z in the mixing zone, the measured PDFs $P(\delta T)$ retain the same characteristic shape as that shown in figure 4(*b*), but they vary slightly with z so that plots of $P(\delta T)$ versus $\delta T/\sigma_T$ do not overlap with each other.

As z is further moved to the bulk region, with the values of z being larger than the cell thickness ($0.1 \lesssim z/D \lesssim 0.4$), the shape of the measured PDFs $P(\delta T)$ changes to another form due to the strong mixing in this region. Figure 4(*c*) shows an example

of the measured $P(\delta T)$ in this region for different values of Ra. The measurements are made at approximately the same position with $z/D \simeq 0.33$. All of the PDFs collapse onto a single curve, which has a Gaussian-like main portion (dashed line) for small temperature fluctuations ($\delta T/\sigma_T \lesssim 1.5$) and an asymmetric tail which smoothly evolves to an exponential shape for large temperature fluctuations ($\delta T/\sigma_T \gtrsim 2.5$).

As z moves toward the central region of the cell ($0.4 \lesssim z/D \lesssim 0.5$), temperature fluctuations become more and more symmetric and so does the measured $P(\delta T)$. Figure 4(*d*) shows the measured PDFs $P(\delta T)$ at the cell centre with different values of Ra. Again, all of the measured PDFs collapse onto a single curve, which is symmetric and has a Gaussian cap (dashed line) for small temperature fluctuations $-2.5 \lesssim \delta T/\sigma_T \lesssim 2.5$ and an exponential-like tail which falls off slower than a Gaussian.

3.2. *Turbulent temperature fluctuations in the $\Gamma = 1$ upright cylinder*

We now examine the scaling properties of the measured $P(\delta T)$ in the $\Gamma = 1$ upright cylinder. Similar to the situation in the thin disk, once δT is normalized by its r.m.s. value σ_T, the temperature PDFs obtained at a fixed value of z and different values of Ra all fall onto a single master curve. Figure 5 shows the measured $P(\delta T)$ as a function of $\delta T/\sigma_T$ for different values of Ra with fixed $Pr = 4.4$ (water). The measurements are made in four representative regions of distance z away from the bottom plate. In each region of z, the measured $P(\delta T)$ has a unique functional form, which remains unchanged with Ra in the Ra range studied. In the inner region of the BL with $z/\delta \lesssim 0.46$, the measured $P(\delta T)$, as shown in figure 5(*a*), can also be well described by the Gaussian function given in (3.1) (dashed line).

In a recent experiment, Wang *et al.* (2018*b*) reported that a mixing zone exists outside the BL in the $\Gamma = 1$ upright cylinder in the range of $0.04 \lesssim z/H \lesssim 0.3$ for $Pr = 4.4$ and $0.06 \lesssim z/H \lesssim 0.3$ for $Pr = 7.6$. Two characteristic forms of $P(\delta T)$ are observed in the mixing zone. Figure 5(*b*) shows a characteristic form of $P(\delta T)$ in the inner region of the mixing zone ($0.04 \lesssim z/H \lesssim 0.07$) for different values of Ra and $Pr \simeq 4.4$. The shape of the measured $P(\delta T)$ in this region is similar to that in the thin disk, namely, all the PDFs have a Gaussian-like main portion (dashed line) for small temperature fluctuations ($\delta T/\sigma_T \lesssim 1$) and a long exponential tail for large temperature fluctuations ($\delta T/\sigma_T \gtrsim 2$). In the outer region of the mixing zone ($0.1 \lesssim z/H \lesssim 0.3$), the measured $P(\delta T)$ has a new characteristic form, which is not observed in the thin disk. Figure 5(*c*) shows an example of the measured $P(\delta T)$ in this region. All of the PDFs for different values of Ra collapse onto a single curve, which has a Gaussian cap (dashed line) for small temperature fluctuations ($-1 \lesssim \delta T/\sigma_T \lesssim 1$) and two asymmetric exponential tails for larger temperature fluctuations. For the tail with $\delta T/\sigma_T \lesssim -1$, it smoothly connects to the Gaussian cap and we believe that it results from the cold plumes passing through the measuring position. There is an abrupt change in the local slope of the measured $P(\delta T)$ between the Gaussian cap and the exponential tail with $\delta T/\sigma_T \gtrsim 2$. This result indicates that the properties of the cold and warm plumes in the outer region of the mixing zone are different.

When z moves into the bulk region ($0.3 \lesssim z/H \lesssim 0.5$), the measured $P(\delta T)$ has a small Gaussian cap with two smooth but asymmetric exponential tails (not shown here). As z moves toward the cell centre ($z/H = 0.5$), the asymmetry between the two exponential tails reduces and finally vanishes at the cell centre. Figure 5(*d*) shows the measured PDFs $P(\delta T)$ at the cell centre for different values of Ra. Except for a small round-off near the origin, all of the PDFs are symmetric and have a long exponential

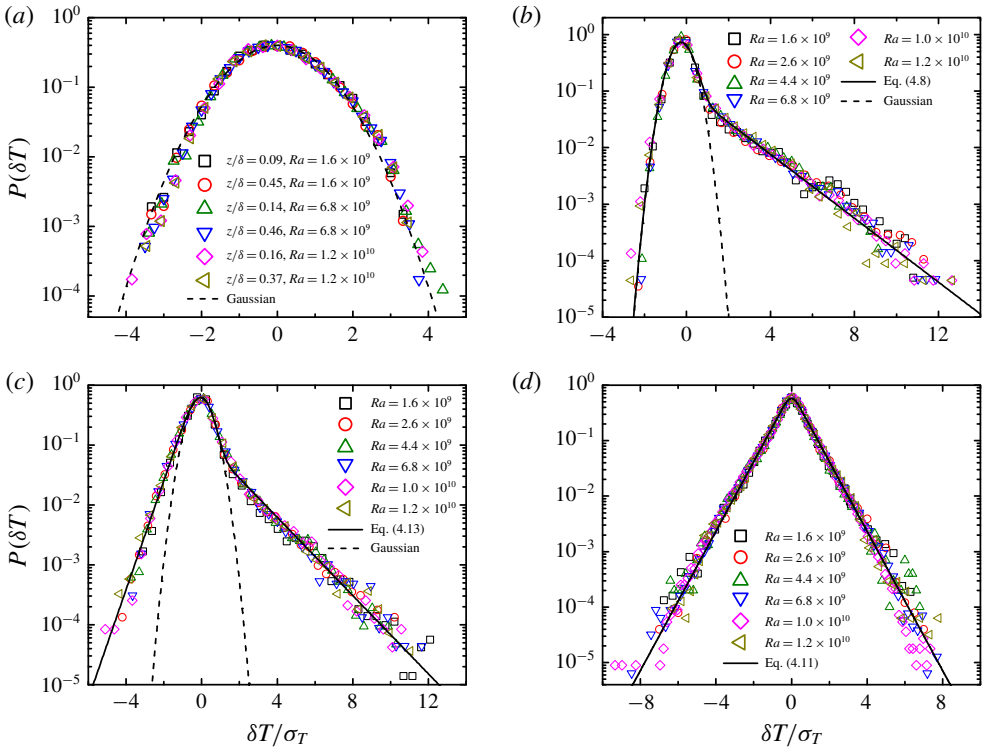

FIGURE 5. (Colour online) Measured PDF $P(\delta T)$ of the normalized temperature fluctuation $\delta T/\sigma_T$ for different values of Ra with a fixed value $Pr = 4.4$ (water). The measurements are made in the $\Gamma = 1$ upright cylinder and in four representative regions of distance z away from the bottom plate centre: (*a*) $z/\delta \lesssim 0.46$ (inner region of the BL), (*b*) $z/H = 0.05$ (inner mixing zone), (*c*) $z/H = 0.16$ (outer mixing zone) and (*d*) $z/H = 0.5$ (cell centre). The dashed lines in (*a–c*) show a Gaussian function given in (3.1). The solid line in (*b*) shows a fit of (4.8) to the data points with $\alpha_1 = 0.31 \pm 0.06$ and $\beta = 0.18 \pm 0.05$. The solid line in (*c*) shows a fit of (4.13) to the data points with $\alpha_1 = 0.33 \pm 0.06$, $\alpha_2 = 0.92 \pm 0.15$ and $\beta = 0.18 \pm 0.05$. The solid line in (*d*) is a fit of (4.11) to the data points with $\alpha = 0.30 \pm 0.06$.

tail (solid line) on each side of the distribution with its amplitude varied by more than 4 decades, which falls off much slower than a Gaussian (Kadanoff 2001). The exponential PDF $P(\delta T)$ was also observed in the previous convection experiments with Ra varied in a wide range from 4×10^7 up to 10^{15} and in various convecting fluids (Castaing *et al.* 1988; Sano *et al.* 1989; Gollub *et al.* 1991; Solomon & Gollub 1991; Belmonte *et al.* 1994; Niemela *et al.* 2000; Du & Tong 2001; Zhou & Xia 2002; He *et al.* 2007; Wei & Ahlers 2016).

Figure 6 shows $P(\delta T)$ as a function of $\delta T/\sigma_T$ for different values of Ra with fixed $Pr = 7.6$ (20 wt.% aqueous solution of glycerin). It is seen that the measured PDFs $P(\delta T)$ in the four representative regions of z for the 20 wt.% glycerin solution have similar behaviours to those as shown in figure 5 for water. At a fixed location z, the measured PDFs $P(\delta T)$ with different values of Ra all fall onto a single master curve, which remains unchanged with Ra in the Ra range studied. The shape of $P(\delta T)$ continuously evolves with z, from a Gaussian form in the inner region

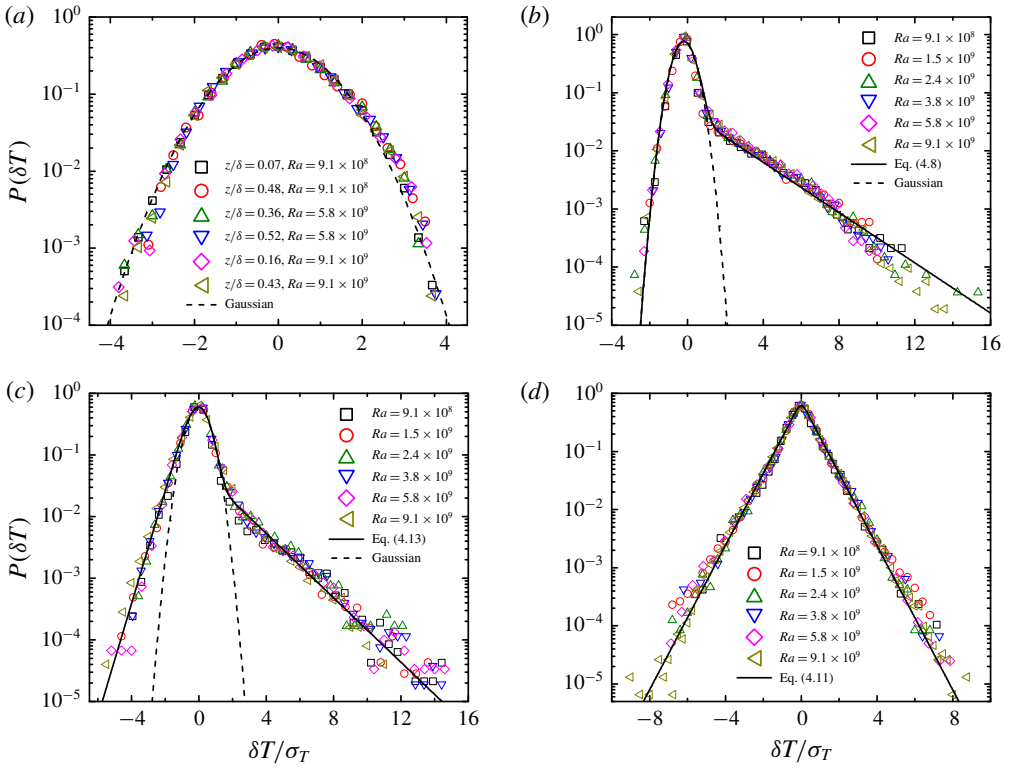

FIGURE 6. (Colour online) Measured PDF $P(\delta T)$ as a function of $\delta T/\sigma_T$ for different values of Ra with a fixed value $Pr = 7.6$ (20 wt.% aqueous solution of glycerin). The measurements are made in the $\Gamma = 1$ upright cylinder and in four representative regions of distance z away from the bottom plate: (*a*) $z/\delta \lesssim 0.52$ (inner region of the BL), (*b*) $z/H = 0.062$ (inner mixing zone), (*c*) $z/H = 0.18$ (outer mixing zone) and (*d*) $z/H = 0.5$ (cell centre). The dashed lines in (*a–c*) show a Gaussian function given in (3.1). The solid line in (*b*) shows a fit of (4.8) to the data points with $\alpha_1 = 0.24 \pm 0.04$ and $\beta = 0.10 \pm 0.03$. The solid line in (*c*) shows a fit of (4.13) to the data points with $\alpha_1 = 0.30 \pm 0.05$, $\alpha_2 = 1.05 \pm 0.2$ and $\beta = 0.10 \pm 0.03$. The solid line in (*d*) is a fit of (4.11) to the data points with $\alpha = 0.20 \pm 0.04$.

of the BL to an exponential form at the cell centre. For the two working fluids used in the experiment, previous studies (Wu & Libchaber 1991; Zhang, Childress & Libchaber 1997; Chillá *et al.* 2004; Ahlers *et al.* 2006*b*) have shown that the non-Oberbeck–Boussinesq (NOB) effect of distilled water is very weak. The 20 wt.% aqueous solution of glycerin, on the other hand, has a stronger NOB effect, as its viscosity depends sensitively on the fluid temperature. It is seen from figures 5 and 6 that the four distinct forms of the measured $P(\delta T)$ in the four flow regions remain approximately the same in the two working fluids, suggesting that the characteristic behaviours of the measured $P(\delta T)$ are not influenced very much by the NOB effect.

4. Further theoretical analysis

Based on the above experimental results, we now derive expressions of the temperature PDF $P(\delta T)$ in different regions. We assume that temperature fluctuations

in the convecting fluid are made from two independent sources, as shown in (1.3). The turbulent background is assumed to be homogeneous, so that $\delta T_B(t)$ is homogeneous both in space and time and has a Gaussian distribution

$$P_B(\delta T_B) = \frac{1}{\sqrt{2\pi}\sigma_B} e^{-\delta T_B^2/(2\sigma_B^2)}, \quad \delta T_B \in (-\infty, +\infty), \tag{4.1}$$

where σ_B is the r.m.s. value of $\delta T_B(t)$. Because thermal plumes have a non-uniform spatial distribution in the convection cell, $\delta T_P(t)$ can be further divided into $\delta T_P^h(t)$ for warm plumes near the bottom conducting plate and $\delta T_P^c(t)$ for cold plumes near the top conducting plate. As mentioned in Introduction, the conditional PDF for temperature fluctuations resulting from thermal plumes alone has a simple exponential form (He *et al.* 2018). Therefore, the PDFs for $\delta T_P^h(t)$ and $\delta T_P^c(t)$ can be expressed, respectively, as

$$P_h(\delta T_P^h) = \frac{1}{\sigma_h} e^{-\delta T_P^h/\sigma_h}, \quad \delta T_P^h \in [0, +\infty) \tag{4.2}$$

and

$$P_c(\delta T_P^c) = \frac{1}{\sigma_c} e^{\delta T_P^c/\sigma_c}, \quad \delta T_P^c \in (-\infty, 0], \tag{4.3}$$

where σ_h and σ_c are, respectively, the r.m.s. value of $\delta T_P^h(t)$ and $\delta T_P^c(t)$. The condition $\delta T_P^h \geqslant 0$ applies for warm plumes and $\delta T_P^c \leqslant 0$ applies for cold plumes, which state that the thermal plumes are fluid particles with their temperature warmer (or colder) than the surroundings.

In the lower half of the bulk region, one finds more warm plumes than cold plumes. In this case, the local temperature fluctuation can be expressed as

$$\delta T(t) \simeq \delta T_B(t) + \delta T_P^h(t), \tag{4.4}$$

and its PDF is a convolution of (4.1) and (4.2) with

$$\begin{aligned} P(\delta T) &= \int_0^{+\infty} P_B(\delta T - \delta T_P^h) P_h(\delta T_P^h)\, \mathrm{d}(\delta T_P^h) \\ &= \frac{1}{2\sigma_h} e^{[(1/2)(\sigma_B/\sigma_h)^2 - \delta T/\sigma_h - 1]} \mathrm{erfc}\left(\frac{\sigma_B^2/\sigma_h - \delta T - \sigma_h}{\sqrt{2}\sigma_B}\right), \end{aligned} \tag{4.5}$$

where $\mathrm{erfc}(x)$ is the complementary error function. Similar convolution was also used in the study of scaler mixing (Le Borgne *et al.* 2017). In (4.5), we have dropped off the mean value of δT so that $P(\delta T)$ has a zero mean. The mean value of δT represents the contribution of thermal plumes to the mean temperature field, which is small but spatially heterogeneous. As the focus of this paper is on local temperature fluctuations, we will not consider the local mean value of δT in the rest of our analysis. From (4.5), one can show that $P(\delta T)$ has a r.m.s. value of $\sigma_T = (\sigma_B^2 + \sigma_h^2)^{1/2}$. With the normalized variable $\xi = \delta T/\sigma_T$, equation (4.5) can be rewritten as

$$P(\xi; \alpha_1) = \sigma_T P(\sigma_T \xi) = \frac{\sqrt{1+\alpha_1^2}}{2} e^{[\alpha_1^2/2 - \xi\sqrt{1+\alpha_1^2} - 1]} \mathrm{erfc}\left(\frac{\alpha_1^2 - \xi\sqrt{1+\alpha_1^2} - 1}{\sqrt{2}\alpha_1}\right), \tag{4.6}$$

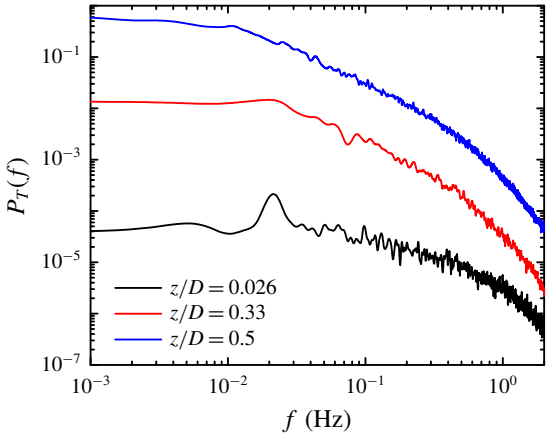

FIGURE 7. (Colour online) Comparison of the measured power spectra $P_T(f)$ of local temperature fluctuations $\delta T(t)$ in three representative regions of distance z away from the bottom plate: $z/D = 0.026$ (mixing zone, black curve), $z/D = 0.33$ (bulk region, red curve) and $z/D = 0.5$ (cell centre, blue curve). The measurements are conducted at $Ra = 5.3 \times 10^9$ and $Pr = 7.6$ in the thin disk. For clarity, the measured $P_T(f)$ is shifted vertically.

where $\alpha_1 = \sigma_B/\sigma_h$. The solid line in figure 4(*c*) shows a fit of (4.6) to the data points with $\alpha_1 = 1.1 \pm 0.2$ as a fitting parameter. Excellent agreement is found between the theoretical prediction and experimental data. The obtained value of $\alpha_1 = 1.1$ suggests that the two fluctuation sources have comparable r.m.s. values in the bulk region of the thin disk.

In the above, the two signals $\delta T_B(t)$ and $\delta T_P^h(t)$ are assumed to be continuous in time. However, this is not always the case. For example, it was reported (Song *et al.* 2011) that warm plumes emit periodically from the lower BL to the mixing zone, so that $\delta T_P^h(t)$ in this region is not continuous in time. Figure 7 shows a comparison of the measured power spectra $P_T(f)$ of $\delta T(t)$ in three representative regions of the thin disk cell. It is seen that in the mixing zone ($z/D = 0.026$), the measured $P_T(f)$ (black curve) reveals a peak at $f \simeq 0.02$ Hz, indicating a periodic emission of warm plumes from the lower BL (Song *et al.* 2011). The frequency peak in $P_T(f)$ gradually diminishes with increasing z and eventually vanishes in the bulk region (red curve) and at the cell centre (blue curve), as a result of turbulent mixing and plume–plume interactions, which smear out the coherence of plume emission. This finding suggests that at certain times t, $\delta T_P^h(t) \simeq 0$ and $\delta T(t) \simeq \delta T_B(t)$. To characterize this temporal intermittency in the mixing zone, we introduce two duty cycle parameters with β being used to describe the probability for $\delta T(t) = \delta T_B(t) + \delta T_P^h(t)$ and $1 - \beta$ for the probability that $\delta T(t) = \delta T_B(t)$. In this case, the PDF of $\delta T(t)$ can be written as

$$\begin{aligned} P(\delta T) &= (1-\beta)P_B(\delta T) + \beta \int_0^{+\infty} P_B(\delta T - \delta T_P^h) P_h(\delta T_P^h)\, \mathrm{d}(\delta T_P^h) \\ &= \frac{1-\beta}{\sqrt{2\pi}\sigma_B} e^{[-(\delta T + \beta\sigma_h)^2/(2\sigma_B^2)]} + \frac{\beta}{2\sigma_h} e^{[(1/2)(\sigma_B/\sigma_h)^2 - \delta T/\sigma_h - \beta]} \mathrm{erfc}\left(\frac{\sigma_B^2/\sigma_h - \delta T - \beta\sigma_h}{\sqrt{2}\sigma_B}\right). \end{aligned} \tag{4.7}$$

In (4.7) $P(\delta T)$ has a r.m.s. value $\sigma_T = (\sigma_B^2 + (2\beta - \beta^2)\sigma_h^2)^{1/2}$. With the normalized variable $\xi = \delta T/\sigma_T$, equation (4.7) can be rewritten as

$$P(\xi;\alpha_1,\beta) = \frac{(1-\beta)\gamma}{\sqrt{2\pi}\alpha_1} e^{[-(\beta+\gamma\xi)^2/(2\alpha_1^2)]} + \frac{\beta\gamma}{2} e^{[\alpha_1^2/2-\gamma\xi-\beta]} \mathrm{erfc}\left(\frac{\alpha_1^2-\gamma\xi-\beta}{\sqrt{2}\alpha_1}\right), \quad (4.8)$$

where $\gamma = (\alpha_1^2 + 2\beta - \beta^2)^{1/2}$.

It is found that the theoretical prediction given in (4.8) can well describe the experimental results in the mixing zone of both the thin disk cell and upright cylinder. The solid line in figure 4(*b*) shows a fit of (4.8) to the data points with $\alpha_1 = 0.25 \pm 0.05$ and $\beta = 0.1 \pm 0.03$ as two fitting parameters. The solid line in figure 5(*b*) shows a fit of (4.8) to the data points in the inner mixing zone of the $\Gamma = 1$ upright cylinder filled with water ($Pr = 4.4$) using $\alpha_1 = 0.31 \pm 0.06$ and $\beta = 0.18 \pm 0.05$ as two fitting parameters. Similarly, the solid line in figure 6(*b*) shows a fit of (4.8) to the data points in the inner mixing zone of the $\Gamma = 1$ upright cylinder filled with the 20 wt. % aqueous solution of glycerin ($Pr = 7.6$) using $\alpha_1 = 0.24 \pm 0.04$ and $\beta = 0.1 \pm 0.03$.

When the measuring position z moves to the cell centre, both warm and cold plumes contribute to temperature fluctuations. In this case, the local temperature fluctuation can be expressed as

$$\delta T(t) = \delta T_B(t) + \delta T_P^h(t) + \delta T_P^c(t), \quad (4.9)$$

and its PDF can be written as

$$\begin{aligned} P(\delta T) &= \int_{-\infty}^{0}\int_{0}^{+\infty} P_B(T - \delta T_P^h - \delta T_P^c) P_h(\delta T_P^h) P_c(\delta T_P^c) \mathrm{d}(\delta T_P^h)\,\mathrm{d}(\delta T_P^c) \\ &= \frac{1}{4\sigma_P} e^{(\sigma_B/\sigma_P)^2/2} \left[e^{\delta T/\sigma_P} \mathrm{erfc}\left(\frac{\sigma_B^2 + \delta T\sigma_P}{\sqrt{2}\sigma_P\sigma_B}\right) + e^{-\delta T/\sigma_P} \mathrm{erfc}\left(\frac{\sigma_B^2 - \delta T\sigma_P}{\sqrt{2}\sigma_P\sigma_B}\right)\right], \end{aligned} \quad (4.10)$$

where $\sigma_P \equiv \sigma_h = \sigma_c$, because the system is symmetric at the cell centre. In (4.10), $P(\delta T)$ has a r.m.s. value $\sigma_T = (\sigma_B^2 + 2\sigma_P^2)^{1/2}$. With the normalized variable $\xi = \delta T/\sigma_T$, equation (4.10) can be rewritten as

$$\begin{aligned} P(\xi;\alpha) &= \frac{\sqrt{\alpha^2+2}}{4} e^{\alpha^2/2} \left[e^{\xi\sqrt{\alpha^2+2}} \mathrm{erfc}\left(\frac{\alpha^2 + \xi\sqrt{\alpha^2+2}}{\sqrt{2}\alpha}\right)\right. \\ &\quad \left. + e^{-\xi\sqrt{\alpha^2+2}} \mathrm{erfc}\left(\frac{\alpha^2 - \xi\sqrt{\alpha^2+2}}{\sqrt{2}\alpha}\right)\right], \end{aligned} \quad (4.11)$$

where $\alpha = \sigma_B/\sigma_P$. Equation (4.11) is a symmetric function of ξ with the exponential distribution ($\alpha = 0$) and Gaussian distribution ($\alpha = +\infty$) being its two asymptotic forms.

It is found that the theoretical prediction given in (4.11) can well describe the experimental results at the centre of both convection cells. The solid line in figure 4(*d*) shows a fit of (4.11) to the data points in the thin disk with $\alpha = 1.7 \pm 0.3$ as a fitting parameter. The solid line in figure 5(*d*) shows a fit of (4.11) to the data points at the centre of the $\Gamma = 1$ upright cylinder filled with water ($Pr = 4.4$) using $\alpha = 0.30 \pm 0.06$.

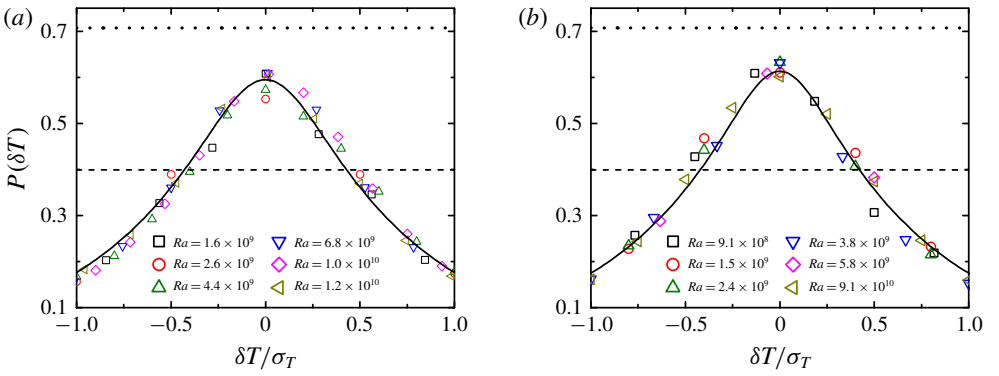

FIGURE 8. (Colour online) Measured temperature PDF $P(\delta T)$ as a function of $\delta T/\sigma_T$ for different values of Ra and at a fixed value of $Pr = 4.4$ (a) and $Pr = 7.6$ (b). The measurements are conducted at the centre of the $\Gamma = 1$ upright cylinder, and the data in (a) and (b) are the same as those shown in figure 5(d) and figure 6(d), respectively. For clarity, the measured PDFs are plotted on a linear scale showing an expanded view of the round-off cap region near $\delta T/\sigma_T \simeq 0$. The solid lines are the fits of (4.11) to the data points with $\alpha = 0.30 \pm 0.06$ (a) and $\alpha = 0.20 \pm 0.04$ (b). The horizontal dashed line shows the expected peak value $1/\sqrt{2\pi}$ for a normalized Gaussian distribution, and the horizontal dotted line shows the expected peak value $1/\sqrt{2}$ for a normalized exponential distribution.

Similarly, the solid line in figure 6(d) shows a fit of (4.11) to the data points at the centre of the $\Gamma = 1$ upright cylinder filled with the 20 wt.% aqueous solution of glycerin ($Pr = 7.6$) using $\alpha = 0.20 \pm 0.04$.

While the effect of background fluctuations at the cell centre is relatively small, it nevertheless provides a measurable mixing effect to smear out the distribution of thermal plumes. Mathematically, a pure exponential distribution has a normalized form, $P(\xi) = (1/\sqrt{2})\exp(-\sqrt{2}|\xi|)$, so that its peak value at $\xi = 0$ is $P_{max} = 1/\sqrt{2} \simeq 0.707$. On the other hand, the peak value of a normalized Gaussian distribution is $P_{max} = 1/\sqrt{2\pi} \simeq 0.399$. Figure 8 shows a magnified view of the measured $P(\delta T)$ near the origin. It is seen that all the measured values of P_{max} for different values of Ra and Pr are in between $1/\sqrt{2}$ (dotted lines) and $1/\sqrt{2\pi}$ (dashed lines), indicating the existence of a Gaussian component. In a physical system, this Gaussian component at the origin precludes the non-analytic sharp peak of the exponential distribution (Wei & Ahlers 2016).

Equation (4.11) can well describe the temperature PDFs obtained not only from the above experiments but also from previous experiments (Wu & Libchaber 1992; Du & Tong 2001). Figure 9 shows the measured $P(\delta T)$ as a function of $\delta T/\sigma_T$ for a low-temperature (5 K) helium gas ($Pr = 0.7$) over a range of Ra. The measurements were conducted at the centre of a $\Gamma = 0.5$ upright cylinder (Wu & Libchaber 1992). The solid line shows a fit of (4.11) to the data points with $\alpha = 1.2 \pm 0.2$ as a fitting parameter. Similar measurements at the centre of a $\Gamma = 6.7$ upright cylinder with $Pr = 0.7$ (Wu & Libchaber 1992) are also found to be well described by (4.11) with $\alpha = 1.5 \pm 0.3$ (not shown here). These results further confirm that our model is quite general and can be used to describe temperature PDFs in a closed convection cell with different aspect ratios and filled with a working fluid with different values of Ra and Pr.

Finally, we consider a general case described in (4.9), in which $\delta T_P^h(t)$ is intermittent with its duty ratio being β. The corresponding PDF $P(\delta T)$ is given as

$$\begin{aligned} P(\delta T) &= (1-\beta)\int_{-\infty}^{\sigma_c} P_B(\delta T-\delta T_P^c)P_c(\delta T_P^c)\,\mathrm{d}(\delta T_P^c) \\ &\quad +\beta\int_{-\infty}^{\sigma_c}\int_{-\sigma_h}^{+\infty} P_B(\delta T-\delta T_P^h-\delta T_P^c)P_h(\delta T_P^h)P_c(\delta T_P^c)\,\mathrm{d}(\delta T_P^h)\,\mathrm{d}(\delta T_P^c) \\ &= \frac{1-\beta}{2\sigma_c}e^{[(\sigma_B/\sigma_c)^2/2+(\delta T+\beta\sigma_h)/\sigma_c-1]}\mathrm{erfc}\left(\frac{\sigma_B^2+(\delta T+\beta\sigma_h-\sigma_c)\sigma_c}{\sqrt{2}\sigma_B\sigma_c}\right) \\ &\quad +\frac{\beta}{2(\sigma_h+\sigma_c)}e^{[(\sigma_B/\sigma_h)^2/2-(\delta T-\sigma_c)/\sigma_h-\beta]}\mathrm{erfc}\left(\frac{\sigma_B^2-(\delta T+\beta\sigma_h-\sigma_c)\sigma_h}{\sqrt{2}\sigma_B\sigma_h}\right) \\ &\quad +\frac{\beta}{2(\sigma_h+\sigma_c)}e^{[(\sigma_B/\sigma_c)^2/2+(\delta T+\beta\sigma_h)/\sigma_c-1]}\mathrm{erfc}\left(\frac{\sigma_B^2+(\delta T+\beta\sigma_h-\sigma_c)\sigma_c}{\sqrt{2}\sigma_B\sigma_c}\right). \end{aligned} \tag{4.12}$$

In (4.12), $P(\delta T)$ has a r.m.s. value $\sigma_T=(\sigma_B^2+\sigma_c^2+(2\beta-\beta^2)\sigma_h^2)^{1/2}$. With the normalized variable $\xi=\delta T/\sigma_T$, equation (4.12) can be rewritten as

$$\begin{aligned} P(\xi;\alpha_1,\alpha_2,\beta) &= \frac{(1-\beta)\gamma_2}{2}e^{[\alpha_2^2/2+\gamma_2\xi+\beta\alpha_2/\alpha_1-1]}\mathrm{erfc}\left(\frac{\alpha_2^2+\gamma_2\xi+\beta\alpha_2/\alpha_1-1}{\sqrt{2}\alpha_2}\right) \\ &\quad +\frac{\beta\alpha_1\gamma_2}{2(\alpha_1+\alpha_2)}e^{[\alpha_1^2/2-\gamma_1\xi+\alpha_1/\alpha_2-\beta]}\mathrm{erfc}\left(\frac{\alpha_1^2-\gamma_1\xi+\alpha_1/\alpha_2-\beta}{\sqrt{2}\alpha_1}\right) \\ &\quad +\frac{\beta\alpha_1\gamma_2}{2(\alpha_1+\alpha_2)}e^{[\alpha_2^2/2+\gamma_2\xi+\beta\alpha_2/\alpha_1-1]}\mathrm{erfc}\left(\frac{\alpha_2^2+\gamma_2\xi+\beta\alpha_2/\alpha_1-1}{\sqrt{2}\alpha_2}\right), \end{aligned} \tag{4.13}$$

with $\alpha_1=\sigma_B/\sigma_h$, $\alpha_2=\sigma_B/\sigma_c$, $\gamma_1=(\alpha_1^2+\alpha_1^2/\alpha_2^2+2\beta-\beta^2)^{1/2}$ and $\gamma_2=(\alpha_2^2+(2\beta-\beta^2)\alpha_2^2/\alpha_1^2+1)^{1/2}$.

Equation (4.13) is the most general form of $P(\delta T/\sigma_T)$ and includes the asymptotic cases given by (4.6), (4.8) and (4.11). In the case $\alpha_2=+\infty$ and $\beta=1$, equation (4.13) reduces to (4.6). In the case $\alpha_2=+\infty$, equation (4.13) reduces to (4.8). In the case $\alpha_1=\alpha_2=\alpha$ and $\beta=1$, equation (4.13) reduces to (4.11). It is found that (4.13) can well describe the measured $P(\delta T)$ in the outer mixing zone of the $\Gamma=1$ upright cylinder, in which cold plumes are continuous (far away from the upper cooling plate and thus lose their intermittency) and warm plumes are highly intermittent (close to the lower heating plate). The solid line in figure 5(*c*) shows a fit of (4.13) to the data points in the outer mixing zone of the $\Gamma=1$ upright cylinder filled with water ($Pr=4.4$) using $\alpha_1=0.33\pm0.06$, $\alpha_2=0.92\pm0.15$ and $\beta=0.18\pm0.05$. Similarly, the solid line in figure 6(*c*) shows a fit of (4.13) to the data points in the outer mixing zone of the $\Gamma=1$ upright cylinder filled with the 20 wt.% aqueous solution of glycerin ($Pr=7.6$) using $\alpha_1=0.30\pm0.05$, $\alpha_2=1.05\pm0.2$ and $\beta=0.10\pm0.03$.

Table 1 gives a summary of the final fitting results obtained in the two convection cells. It is seen that the fitted values of $\alpha_1=\sigma_B/\sigma_h$ in the thin disk cell increase monotonically, as the measuring position z moves from the mixing zone to the cell centre (see figure 3). This result suggests that the contribution of warm plumes to the local temperature fluctuations decreases with increasing z, as expected. However, the

https://doi.org/10.1017/jfm.2019.405 Published online by Cambridge University Press

Flow region		Upright cylinder ($Pr = 4.4$)			Upright cylinder ($Pr = 7.6$)			Thin disk ($Pr = 7.6$)		
		α_1	α_2	β	α_1	α_2	β	α_1	α_2	β
Mixing zone	Inner	0.31 ± 0.06	$+\infty$	0.18 ± 0.05	0.24 ± 0.04	$+\infty$	0.1 ± 0.03	0.25 ± 0.05	$+\infty$	0.1 ± 0.03
	Outer	0.33 ± 0.06	0.92 ± 0.15	0.18 ± 0.05	0.30 ± 0.05	1.05 ± 0.2	0.1 ± 0.03			
Turbulent bulk		0.30 ± 0.06	0.33 ± 0.06	1	0.23 ± 0.05	0.26 ± 0.05	1	1.1 ± 0.2	$+\infty$	1
Cell centre		0.30 ± 0.06	0.30 ± 0.06	1	0.20 ± 0.04	0.20 ± 0.04	1	1.7 ± 0.3	1.7 ± 0.3	1

TABLE 1. Obtained values of the parameters α_1, α_2 and β in (4.13) for three different flow regions in the two convection cells. The numbers with an error bar indicate the fitted values with a fitting uncertainty and those without an error bar are the expected values in theory.

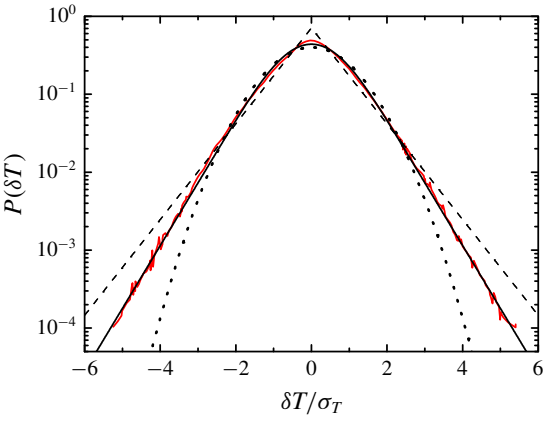

FIGURE 9. (Colour online) Measured temperature PDF $P(\delta T)$ as a function of $\delta T/\sigma_T$ at the centre of a $\Gamma = 0.5$ upright cylinder (red line). The measurements were conducted at a fixed value of $Pr = 0.7$ (a low-temperature helium gas) in the Ra range from 4×10^9 to 6×10^{14}. The data are taken from figure 1(b) in Wu & Libchaber (1992). The solid line shows a fit of (4.11) to the data points with $\alpha = 1.2 \pm 0.2$. The dashed and dotted lines show, respectively, a simple exponential distribution function and a Gaussian distribution function for comparison.

fitted values of α_1 in the upright cylinder do not change much in the three different flow regions. The fitted values of α_1 in the turbulent bulk region and at the centre of the upright cylinder are much smaller than those obtained in the thin disk. These findings indicate that the effect of thermal plumes in the upright cylinder is much larger than that in the thin disk. This is because the quasi-two-dimensional LSC in the thin disk is more stable than the LSC in the upright cylinder, which gives rise to a more organized spatial distribution of thermal plumes, reducing their probabilities to go through the bulk region. Such an aspect-ratio-dependent $P(\delta T)$ at the cell centre was also reported previously by Solomon & Gollub (1991).

It is also seen that the fitted value of β at $Pr = 7.6$ is $\beta = 0.1$, which indicates that the warm plumes are active for only 10 % of the measuring time, so that they are highly intermittent in the mixing zone. The fact that the obtained value of β in the thin disk is the same as that in the upright cylinder suggests that the fitted value of $\beta = 0.1$ is not sensitive to the changes of cell geometry and Ra. Table 1 also reveals that the fitted values of α_1 and β in the upright cylinder decrease slightly with increasing Pr. This is because the thermal plumes in the mixing zone become more coherent with increasing Pr. Here 'coherent' has two meanings. First, because the warm plumes at larger Pr have a longer lifetime, they are relatively hotter than the warm plumes at lower Pr (at the same position z). As a result, the plume-induced temperature fluctuations have a larger amplitude, leading to a smaller value of α_1 at larger Pr. Second, because the thermal plumes at larger Pr are more localized in space (less thermal diffusion) and move faster (more buoyant), they have a shorter time passing through the temperature probe and thus a smaller value of β.

5. Summary

We have carried out a systematic study of spatial variations of the PDF $P(\delta T)$ for temperature fluctuations δT in turbulent Rayleigh–Bénard convection. The local

temperature measurements were made along the central axis of two closed convection cells: one is a thin circular disk cell and the other is an upright cylinder of aspect ratio unity. In the experiment, the Rayleigh number Ra was varied in the range between 9×10^8 and 1.2×10^{10} with two fixed Prandtl numbers $Pr = 4.4$ and $Pr = 7.6$. The measured $P(\delta T)$ reveals distinct changes in four different flow regions in the lower half of the cell, namely, the thermal BL near the bottom conducting place, mixing zone outside the BL, lower turbulent bulk region and cell centre. Because of the symmetry of the cell shape, one expects that similar regions exist in the upper half of the cell. These distinct changes in the functional form of $P(\delta T)$ remain unchanged for different values of Ra and Pr, once the normalized temperature fluctuation $\delta T/\sigma_T$ is used as the scaling variable. Here σ_T is the r.m.s. value of δT.

In the inner region of the BL, where the mean temperature gradient remains approximately constant, the measured $P(\delta T)$ has a Gaussian form in both convection cells. In the mixing zone outside the BL, the measured $P(\delta T)$ in the thin disk cell has a Gaussian shape in the main body but with an exponential tail for large positive values of $\delta T/\sigma_T$. Such an exponential tail is caused by the periodic emission of warm plumes from the bottom BL, which also gives rise to an abrupt change in the local slope of the measured exponential tail of $P(\delta T)$. A similar $P(\delta T)$ is also found in the upright cylinder. In the outer region of the mixing zone, the measured $P(\delta T)$ in the upright cylinder evolves to a new shape containing two asymmetric exponential tails for large absolute values of $\delta T/\sigma_T$. This new shape of $P(\delta T)$ is not observed in the thin disk cell. In the lower turbulent bulk region of both convection cells, the abrupt change in the local slope of the measured exponential tail of $P(\delta T)$ disappears, suggesting that the effect of the periodic emission of thermal plumes is diminished. In this case, the measured $P(\delta T)$ in the thin disk has a Gaussian shape in the main body and a smooth exponential tail for large positive values of $\delta T/\sigma_T$. The measured $P(\delta T)$ in the upright cylinder has a Gaussian cap and two asymmetric but smooth exponential tails for large absolute values of $\delta T/\sigma_T$. At the centre of both convection cells, because of the symmetry of the convection cell, the measured $P(\delta T)$ has a symmetric shape with a Gaussian cap for small absolute values of $\delta T/\sigma_T$ and two long exponential tails for large absolute values of $\delta T/\sigma_T$.

Based on the above experimental findings, we proposed a theoretical model which assumes that temperature fluctuations in different regions of the convection cell are all made from two independent sources, namely, a homogeneous background which obeys Gaussian statistics and non-uniform thermal plumes with an exponential distribution. As a result, the temperature PDF $P(\delta T)$ is uniquely described by a convolution of the two modes of fluctuations with a relative strength, which varies among the four different flow regions. The predicted analytic expressions of $P(\delta T)$, as shown in (4.6), (4.8), (4.11) and (4.13), agree well with the experimental results obtained in the present experiment and also in previous experiments. Our model thus provides a unique theoretical framework with a common set of parameters to quantitatively describe the effect of turbulent background, thermal plumes and their spatio-temporal intermittency on the temperature PDF $P(\delta T)$. Such an understanding of turbulent fluctuations with decomposition of fluctuation modes based on the coherent structures in the flow is very useful not only for the study of temperature fluctuations in turbulent thermal convection but also for the understanding of turbulent mixing problems of practical interest.

Acknowledgements

This work was supported in part by the Hong Kong Research Grants Council under grant nos 16306418 (P.T.) and 16302718 (P.T.). X.H. acknowledges the support of

the National Natural Science Foundation of China under grant no. 11772111 and Shenzhen Startup Funds no. CB11409001 and Shenzhen Overseas Talent Project no. CB24405026.

REFERENCES

AHLERS, G., BROWN, E. & NIKOLAENKO, A. 2006*a* Search for slow transients, and the effect of imperfect vertical alignment, in turbulent Rayleigh–Bénard convection. *J. Fluid Mech.* **557**, 347–367.

AHLERS, G., BROWN, E., ARAUJO, F. F., FUNFSCHILLING, D., GROSSMANN, S. & LOHSE, D. 2006*b* Non-Oberbeck-Boussinesq effects in strongly turbulent Rayleigh–Bénard convection. *J. Fluid Mech.* **569**, 409–445.

ARNÈODO, A., BENZI, R., BERG, J., BIFERALE, L., BODENSCHATZ, E., BUSSE, A., CALZAVARINI, E., CASTAING, B., CENCINI, M., CHEVILLARD, L. *et al.* 2008 Universal intermittent properties of particle trajectories in highly turbulent flows. *Phys. Rev. Lett.* **100**, 254504.

ASHKENAZI, S. & STEINBERG, V. 1999 Spectra and statistics of velocity and temperature fluctuations in turbulent convection. *Phys. Rev. Lett.* **83**, 4760–4763.

BELMONTE, A., TILGNER, A. & LIBCHABER, A. 1994 Temperature and velocity boundary layers in turbulent convection. *Phys. Rev.* E **50**, 269–279.

BENZI, R., CILIBERTO, S., TRIPICCIONE, R., BAUDET, C., MASSAIOLI, F. & SUCCI, S. 1993 Extended self-similarity in turbulent flows. *Phys. Rev.* E **48**, R29–R32.

BENZI, R., TRIPICCIONE, R., MASSAIOLI, F., SUCCI, S. & CILIBERTOI, S. 1994 On the scaling of the velocity and temperature structure functions in Rayleigh–Bénard convection. *Europhys. Lett.* **25**, 341–346.

BIFERALE, L. & PROCACCIA, I. 2005 Anisotropy in turbulent flows and in turbulent transport. *Phys. Rep.* **414**, 43–164.

CALZAVARINI, E., TOSCHI, F. & TRIPICCIONE, R. 2002 Evidences of Bolgiano-Obhukhov scaling in three-dimensional Rayleigh–Bénard convection. *Phys. Rev.* E **66**, 016304.

CAMUSSI, R. & VERZICCO, R. 2004 Temporal statistics in high Rayleigh number convective turbulence. *Eur. J. Mech. (*B*/Fluids)* **23**, 427–442.

CAO, N. & CHEN, S. 1997 An intermittency model for passive-scalar turbulence. *Phys. Fluids* **9**, 1203–1205.

CAO, N., CHEN, S. & SREENIVASAN, K. R. 1996 Scalings of low-order structure functions in fluid turbulence. *Phys. Rev. Lett.* **77**, 3799–3802.

CASTAING, B., GUNARATNE, G., HESLOT, F., KADANOFF, L., LIBCHABER, A., THOMAE, S., WU, X.-Z., ZALESKI, S. & ZANETTI, G. 1988 Scaling of hard thermal turbulence in Rayleigh–Bénard convection. *J. Fluid Mech.* **204**, 1–30.

CHERTKOV, M., FALKOVICH, G., KOLOKOLOV, I. & LEBEDEV, V. 1995 Normal and anomalous scaling of 4He fourth-order correlation function of a randomly advected passive scalar. *Phys. Rev.* E **52**, 4924–4941.

CHILLÁ, F., RASTELLO, M., CHAUMAT, S. & CASTAING, B. 2004 Long relaxation times and tilt sensitivity in Rayleigh–Bénard turbulence. *Eur. Phys. J.* B **40**, 223–227.

CHILLÁ, F. & SCHUMACHER, J. 2012 New perspectives in turbulent Rayleigh–Bénard convection. *Eur. Phys. J.* E **35**, 58.

CHING, E. S. C. 2007 Measured thermal dissipation field in turbulent Rayleigh–Bénard convection. *Phys. Rev.* E **75**, 056302.

CHING, E. S. C. & CHAU, K. L. 2001 Scaling laws in the central region of confined turbulent thermal convection. *Phys. Rev.* E **63**, 047303.

CHING, E. S. C., GUO, H. & LO, T. S. 2008 Refined similarity hypotheses in shell models of homogeneous turbulence and turbulent convection. *Phys. Rev.* E **78**, 026303.

CIONI, S., CILIBERTO, S. & SOMMERIA, J. 1995 Temperature structure functions in turbulent convection at low Prandtl number. *Europhys. Lett.* E **32**, 413–418.

DIMOTAKIS, P. E. 2005 Tubulent mixing. *Annu. Rev. Fluid Mech.* **37**, 329–356.

DU, Y.-B. & TONG, P. 2001 Temperature fluctuations in a convection cell with rough upper and lower surfaces. *Phys. Rev.* E **63**, 046303.

GAWĘDZKI, K. & KUPIAINEN, A. 1995 Anomalous scaling of the passive scalar. *Phys. Rev. Lett.* **75**, 3834–3837.

GOLLUB, J. P., CLARKE, J., GHARIB, M., LANE, B. & MESQUITA, O. N. 1991 Fluctuations and transport in a stirred fluid with a mean gradient. *Phys. Rev. Lett.* **67**, 3507–3510.

GROSSMANN, S. & LOHSE, D. 1992 Scaling in hard turbulent Rayleigh–Bénard flow. *Phys. Rev.* A **46**, 903–917.

GROSSMANN, S. & LOHSE, D. 1993 Characteristic scales in Rayleigh–Bénard turbulence. *Phys. Lett.* A **173**, 58–62.

GROSSMANN, S. & LOHSE, D. 2004 Fluctuations in turbulent Rayleigh–Bénard convection: the role of plumes. *Phys. Fluids* **16**, 4462–4472.

HE, X.-Z., CHING, E. S. C. & TONG, P. 2011 Locally averaged thermal dissipation rate in turbulent thermal convection: a decomposition into contributions from different temperature gradient components. *Phys. Fluids* **23**, 025106.

HE, X.-Z., SHANG, X.-D. & TONG, P. 2014 Test of the anomalous scaling of passive temperature fluctuations in turbulent Rayleigh–Bénard convection with spatial inhomogeneity. *J. Fluid Mech.* **753**, 104–130.

HE, X.-Z. & TONG, P. 2009 Measurements of the thermal dissipation field in turbulent Rayleigh–Bénard convection. *Phys. Rev.* E **79**, 026306.

HE, X.-Z., TONG, P. & XIA, K.-Q. 2007 Measured thermal dissipation field in turbulent Rayleigh–Bénard convection. *Phys. Rev. Lett.* **98**, 144501.

HE, X.-Z., WANG, Y. & TONG, P. 2018 Dynamic heterogeneity and conditional statistics of non-Gaussian temperature fluctuations in turbulent thermal convection. *Phys. Rev. Fluids.* **3**, 052401.

ISHIHARA, T., GOTOH, T. & KANEDA, Y. 2009 Study of high-Reynolds number isotropic turbulence by direct numerical simulation. *Annu. Rev. Fluid Mech.* **41**, 165–180.

KADANOFF, L. P. 2001 Turbulent heat flow: structures and scaling. *Phys. Today* **54** (8), 34–39.

KERR, R. 1996 Rayleigh number scaling in numerical convection. *J. Fluid Mech.* **310**, 139–179.

LE BORGNE, T., HUCK, P. D., DENTZ, M. & VILLERMAUX, E. 2017 Scalar gradients in stirred mixtures and the deconstruction of random fields. *J. Fluid Mech.* **812**, 578–610.

LOHSE, D. & XIA, K.-Q. 2010 Small-scale properties of turbulent Rayleigh–Bénard convection. *Annu. Rev. Fluid Mech.* **42**, 335–364.

MASHIKO, T., TSUJI, Y., MIZUNO, T. & SANO, M. 2004 Instantaneous measurement of velocity fields in developed thermal turbulence in mercury. *Phys. Rev.* E **69**, 036306.

NAERT, A., CASTAING, B., CHABAUD, B., HTBRAL, B. & PEINKE, J. 1998 Conditional statistics of velocity fluctuations in turbulence. *Physica* D **113**, 73–78.

NIEMELA, J. J., SKRBEK, L., SREENIVASAN, K. R. & DONNELLY, R. J. 2000 Turbulent convection at very high Rayleigh numbers. *Nature* **404**, 837–840.

OTTINO, J. M. 1989 *The Kinematics of Mixing: Stretching, Chaos, and Transport*. Cambridge University Press.

PAUL, E. L., ATIEMO-OBENG, V. A. & KRESTA, S. M. 2004 *Handbook of Industrial Mixing: Science and Practice*. Wiley.

PROCACCIA, I., CHING, E., CONSTANTIN, P., KADANOFF, L. P., LIBCHABER, A. & WU, X.-Z. 1991 Transitions in convective turbulence: the role of thermal plumes. *Phys. Rev.* A **44**, 8091–8102.

PROCACCIA, I. & ZEITAK, R. 1989 Scaling exponents in nonisotropic convective turbulence. *Phys. Rev. Lett.* **62**, 2128–2131.

PROCACCIA, I. & ZEITAK, R. 1990 Scaling exponents in thermally driven turbulence. *Phys. Rev.* A **42**, 821–830.

QIU, X.-L. & TONG, P. 2001 Large-scale velocity structures in turbulent thermal convection. *Phys. Rev.* E **64**, 036304.

SANO, M., WU, X.-Z. & LIBCHBER, A. 1989 Turbulence in helium-gas free convection. *Phys. Rev.* A **40**, 6421–6430.

SHANG, X.-D., QIU, X.-L., TONG, P. & XIA, K.-Q 2003 Measured local heat transport in turbulent Rayleigh–Bénard convection. *Phys. Rev. Lett.* **90**, 074501.

SHE, Z.-S. & LÉVEQUE, E. 1994 Universal scaling laws in fully developed turbulence. *Phys. Rev. Lett.* **72**, 336–339.

SHE, Z.-S. & ORSZAG, S. A. 1991 Physical model of intermittency: inertial-range non-Gaussian statistics. *Phys. Rev. Lett.* **66**, 1701–1704.

SHRAIMAN, B. I. & SIGGIA, E. D. 1995*a* Anomalous scaling of a passive scalar in turbulent flow. *C. R. Acad. Sci. Paris* **321**, 279–284.

SHRAIMAN, B. I. & SIGGIA, E. D. 1995*b* Scalar turbulence. *Nature* **405**, 639–646.

SIGGIA, E. D. 1994 High Rayleigh number convection. *Annu. Rev. Fluid Mech.* **26**, 137–168.

SKRBEK, L., NIEMELA, J. J., SREENIVASAN, K. R. & DONNELLY, R. J. 2002 Temperature structure functions in the Bolgiano regime of thermal convection. *Phys. Rev.* E **66**, 036303.

SOLOMON, T. H. & GOLLUB, J. P. 1991 Thermal boundary layers and heat flux in turbulent convection: the role of recirculating flows. *Phys. Rev.* A **43**, 6683–6693.

SONG, H., VILLERMAUX, E. & TONG, P. 2011 Coherent oscillations of turbulent Rayleigh–Bénard convection in a thin vertical disk. *Phys. Rev. Lett.* **106**, 184504.

SREENIVASAN, K. R. 1991 Fractals and multifractals in fluid turbulence. *Annu. Rev. Fluid Mech.* **233**, 539–600.

SREENIVASAN, K. R. 1991 On local isotropy of passive scalars in turbulent shear flows. *Proc. R. Soc. Lond.* A **434**, 165–182.

SREENIVASAN, K. R., RAMSHANKAR, R. & MENEVEAU, C. 1989 Mixing, entrainment and fractal dimensions of surfaces in turbulent flows. *Proc. R. Soc. Lond.* A **421**, 79–108.

TAKESHITA, T., SEGAWA, T., GLAZIER, J. A. & SANO, M. 1996 Thermal turbulence in mercury. *Phys. Rev. Lett.* **76**, 1465–1468.

TONG, P. & SHEN, Y. 1992 Relative velocity fluctuations in turbulent Rayleigh–Bénard convection. *Phys. Rev. Lett.* **69**, 2066–2069.

VILLERMAUX, E. 2012 On dissipation in stirred mixtures. *Adv. Appl. Mech.* **45**, 91–107.

WANG, Y., HE, X.-Z. & TONG, P. 2016 Boundary layer fluctuations and their effects on mean and variance temperature profiles in turbulent Rayleigh–Bénard convection. *Phys. Rev. Fluids* **1**, 082301.

WANG, Y., LAI, P.-Y., SONG, H. & TONG, P. 2018*a* Mechanism of large-scale flow reversals in turbulent thermal convection. *Sci. Adv.* **4**, 7480.

WANG, Y., XU, W., HE, X.-Z., YIK, H.-F., WANG, X.-P., SCHUMACHER, J. & TONG, P. 2018*b* Boundary layer fluctuations in turbulent Rayleigh–Bénard convection. *J. Fluid Mech.* **840**, 408–431.

WARHAFT, Z. 2000 Passive scalars in turbulent flows. *Annu. Rev. Fluid Mech.* **32**, 203–240.

WEI, P. & AHLERS, G. 2016 On the nature of fluctuations in turbulent Rayleigh–Bénard convection at large Prandtl numbers. *J. Fluid Mech.* **802**, 203–244.

WILCZEK, M. 2016 Non-Gaussianity and intermittency in an ensemble of Gaussian fields. *New J. Phys.* **18**, 125009.

WU, X.-Z., KADANOFF, L. P., LIBCHABER, A. & SANO, M. 1990 Frequency power spectrum of temperature fluctuations in free convection. *Phys. Rev. Lett.* **64**, 2140–2143.

WU, X.-Z. & LIBCHABER, A. 1992 Scaling relations in thermal turbulence: the aspect-ratio dependence. *Phys. Rev.* A **45**, 842–845.

WU, X.-Z. & LIBCHABER, A. 1991 Non-Boussinesq effects in free thermal convection. *Phys. Rev.* A **43**, 2833–2839.

ZHANG, J., CHILDRESS, S. & LIBCHABER, A. 1997 Non-Boussinesq effect: thermal convection with broken symmetry. *Phys. Fluids* **9**, 1034–1042.

ZHOU, Q. & XIA, K.-Q. 2013 Thermal boundary layer structure in turbulent Rayleigh–Bénard convection in a rectangular cell. *J. Fluid Mech.* **721**, 199–224.

ZHOU, S.-Q. & XIA, K.-Q. 2001 Scaling properties of the temperature field in convective turbulence. *Phys. Rev. Lett.* **87**, 064501.

ZHOU, S.-Q. & XIA, K.-Q. 2002 Plume statistics in thermal turbulence: mixing of an active scalar. *Phys. Rev. Lett.* **89**, 184502.